How to cite: *Angew. Chem. Int. Ed.* **2021**, *60*, 27095 – 27101
International Edition: doi.org/10.1002/anie.202112398
German Edition: doi.org/10.1002/ange.202112398

Single Atom Catalysis

Water Splitting by C_{60}-Supported Vanadium Single Atoms

Gao-Lei Hou, Tao Yang,* Mengyang Li, Jan Vanbuel, Olga V. Lushchikova, Piero Ferrari, Joost M. Bakker, and Ewald Janssens**

Abstract: *Water splitting is an important source of hydrogen, a promising future carrier for clean and renewable energy. A detailed understanding of the mechanisms of water splitting, catalyzed by supported metal atoms or nanoparticles, is essential to improve the design of efficient catalysts. Here, we report an infrared spectroscopic study of such a water splitting process, assisted by a C_{60} supported vanadium atom, $C_{60}V^+ + H_2O \rightarrow C_{60}VO^+ + H_2$. We probe both the entrance channel complex $C_{60}V^+(H_2O)$ and the end product $C_{60}VO^+$, and observe the formation of H_2 as a result from resonant infrared absorption. Density functional theory calculations exploring the detailed reaction pathway reveal that a quintet-to-triplet spin crossing facilitates the water splitting reaction by C_{60}-supported V^+, whereas this reaction is kinetically hindered on the isolated V^+ ion by a high energy barrier. The C_{60} support has an important role in lowering the reaction barrier with more than 70 kJ mol^{-1} due to a large orbital overlap of one water hydrogen atom with one carbon atom of the C_{60} support. This fundamental insight in the water splitting reaction by a C_{60}-supported single vanadium atom showcases the importance of supports in single atom catalysts by modifying the reaction potential energy surface.*

Introduction

Looking for sustainable and environment-friendly alternatives to fossil fuels has become a grand challenge worldwide, which has stimulated extensive efforts to develop efficient energy conversion technologies. As a convenient, safe, and versatile fuel source, hydrogen can be converted to a desired form of energy without the emission of greenhouse gases and pollutants.[1] One important hydrogen source that can be utilized on a large scale is the hydrogen evolution reaction, in which water splitting is an important step.[2] The energy barrier of water splitting is high and needs to be reduced by an appropriate catalyst to strongly increase the reaction rate. A fundamental understanding of the underlying water splitting mechanism is beneficial to guide the design of novel efficient catalysts, and much effort has been devoted to this aim.[3]

In recent years, single-atom catalysis has emerged as a new frontier in heterogeneous catalysis.[4] Single-atom catalysts (SACs), which contain dispersed isolated metal atoms on an otherwise inert support, were first coined in 2011 by Zhang and co-workers, for the CO oxidation reaction using Pt_1/FeO_x.[5] It has been shown that SACs possess several exceptional properties, such as high atomic efficiency, excellent stability, high tunable activity, and high selectivity, lending a promising future to produce efficient catalysts for water splitting. To exhibit high stability and superior reactivity, the dispersed metal atoms have to be embedded or adsorbed at specific sites of the support, emphasizing the importance of the support environment, including surface conditions, support types, and metal–support interactions.[4d–f] First-principles calculations have been employed to investigate the coordination environment, reactivity, and metal–support interactions of SACs, as well as their intrinsic thermodynamic and kinetic stability.[4c,d] For example, using large-scale *ab initio* molecular dynamics (AIMD) simulations, Wang et al. uncovered an enhanced CO oxidation activity if Au atoms (temporarily) escape from a supported Au nanoparticle, showing interesting dynamic catalytic behavior.[6] Recently, high-efficiency water-splitting single-atom electrocatalysts, consisting of precious metals on various supports, such as metal oxides, (doped) mesoporous carbon, MoS_2 nanosheets, and boron monolayers, with superior activity and stability have been developed.[7] However, it is in practice still far from trivial to predict the properties and to guide the design of highly stable and reactive SACs, due to the complexity involved in realistic reaction conditions and the lack of molecular-level understanding of the metal–support interactions and the roles of the supports.

Well-defined isolated clusters with specific size, charge state, and composition, are ideal model systems to obtain insight at the molecular level into elementary steps relevant to many catalytic processes, including water activation and splitting.[8] For instance, Lang et al. studied the reactivity of a series of $Mn_xO_y^+$ and $Ca_nMn_{4-n}O_4^+$ clusters towards H_2O, and found that only certain cluster sizes and compositions can dehydrogenate H_2O and unveiled the specific roles played by

[*] G.-L. Hou, J. Vanbuel, P. Ferrari, E. Janssens
Quantum Solid-State Physics, Department of Physics and Astronomy, KU Leuven
Celestijnenlaan 200D, 3001 Leuven (Belgium)
E-mail: chemglhou@gmail.com
ewald.janssens@kuleuven.be

G.-L. Hou, T. Yang, M. Li
MOE Key Laboratory for Non-Equilibrium Synthesis and Modulation of Condensed Matter, School of Physics, Xi'an Jiaotong University
Xi'an, 710049 (P. R. China)
E-mail: taoyang1@xjtu.edu.cn

O. V. Lushchikova, J. M. Bakker
Radboud University, Institute for Molecules and Materials, FELIX Laboratory
Toernooiveld 7, 6525 ED Nijmegen (The Netherlands)

Supporting information (experimental and theoretical methods, additional experimental and theoretical results, and Cartesian coordinates of the computed structures) and the ORCID identification number(s) for the author(s) of this article can be found under https://doi.org/10.1002/anie.202112398.

calcium atoms.[9] Asmis and co-workers found that water adsorbs dissociatively on the $Al_3O_4^+$ cluster, forming hydroxyl.[10] Recently, Bowen and co-workers reported that single platinum and nickel anions can activate water, leading to water-activated $HMOH^-$ (M = Pt and Ni) intermediates.[11] In recent studies on the reaction between water and both cationic and neutral vanadium clusters, Zhang et al. found that three-atom vanadium clusters, $V_3^{+/0}$, can greatly reduce the energy barrier of the critical step towards effective H_2 release from a single water molecule compared to a single vanadium atom.[8g,j] This finding is consistent with infrared spectroscopic studies under quite similar experimental conditions of $V^+(H_2O)_n$, which indicate that the water molecules on free V^+, in particular for $n=1$, remain intact.[12] Of course, in neither experiment the presence of excited state V^+ species can be ruled out; it is well-documented, both experimentally and theoretically, that the a^3F exited state reacts more efficiently than the a^5D ground state in forming VO^+ and H_2 products.[13] In Fourier-transform ion cyclotron resonance mass spectrometry (FTICR-MS) experiments, which have considerably longer time scales, $V^+(H_2O)_n$ ($n=1$–41) clusters have been observed to release H and/or H_2, due to blackbody radiation[14] and UV photoexcitation.[15] Although these studies provide important understanding about the interactions of water with isolated metal atoms and clusters, they are generally far from the reality of SACs that contain both metals and supports.

In this work, we synthesized a $C_{60}V^+$ complex via laser vaporization and investigated its properties as a vanadium SAC with C_{60} acting as a model for carbon-based supports. C_{60} has unique physical, chemical, and mechanical properties, and can be regarded as a small piece of well-defined porous carbon materials, such as graphene and carbon nanotubes, although it is slightly more irregular due to the presence of both hexagons and pentagons.[4d] Recently, carbon nanomaterials with intrinsic pentagonal defects and curvatures have emerged as novel materials for various catalytic applications.[16] Having synthesized $C_{60}V^+$, we reacted it with H_2O, and subsequently employed infrared multiple photon dissociation (IRMPD) spectroscopy to characterize both the entrance channel complex $C_{60}V^+(H_2O)$ and the end product $C_{60}VO^+$ of the $C_{60}V^+ + H_2O \rightarrow C_{60}V^+(H_2O) \rightarrow C_{60}VO^+ + H_2$ reaction. The reaction mechanism, metal–support interactions, and support effects are investigated by density functional theory (DFT) calculations, and compared with reactions between the isolated V^+ and water.[13] Our study showcases the crucial role of the support in lowering the reaction barrier, which in this particular case occurs via orbital overlap of a carbon atom with one of the water hydrogen atoms during the abstraction reaction.

Results and Discussion

Figure 1a presents the mass distributions of $C_{60}V^+$, $C_{60}VO^+$, and $C_{60}V^+(H_2O)$ produced in a laser vaporization source, with (red) and without (black) IR irradiation at 1030 cm^{-1}. Full mass spectra showing the different complexes produced in the experiments can be found in Figure S1 in the Supporting Information. $C_{60}VO^+$ was produced either due to the partially oxidized vanadium target or by the presence of trace amounts of oxygen or water in the gas inlet, while $C_{60}V^+(H_2O)$ was produced due to a trace amount of water in the helium carrier gas (see experimental details in the Supporting Information). The simulated natural isotope distributions of $C_{60}VO^+$ (blue sticks) and $C_{60}V^+(H_2O)$ (pink sticks) reproduce the mass patterns (inset of Figure 1a), indicating a faithful mass assignment. The isotopic mass overlap between $C_{60}VO^+$ and $C_{60}V^+(H_2O)$ is limited and the overall contribution of $C_{60}VO^+$ to $C_{60}V^+(H_2O)$ is estimated to be approximately 5%.

It can be seen from Figure 1a that upon IR irradiation at 1030 cm^{-1}, both $C_{60}VO^+$ and $C_{60}V^+(H_2O)$ decrease in intensity. For $C_{60}VO^+$, since VO^+ has a large binding energy of 584 kJ mol^{-1},[17] the most plausible infrared induced dissociation channel is $C_{60}VO^+ \rightarrow C_{60} + VO^+$ with a calculated dissociation energy of 254 kJ mol^{-1}. For $C_{60}V^+(H_2O)$, the naturally anticipated dissociation channels include

$$C_{60}V^+(H_2O) \rightarrow C_{60}V^+ + H_2O \quad (1)$$

$$C_{60}V^+(H_2O) \rightarrow C_{60} + V^+(H_2O) \quad (2)$$

The calculated dissociation energies of these dissociation channels are 116 and 193 kJ mol^{-1}, respectively. Since water loss requires a much lower energy, it is anticipated that the most probable channel seen in Figure 1a is reaction (1). Evidence for this is found in the observed intensity increase of $C_{60}V^+$. Note that the first two isotopic peaks of $C_{60}V^+$ ($m/z=$ 771 and 772 amu) are saturated because their intensities exceed the data acquisition window; the increase is more clearly visible for the $m/z=773$ and 774 amu isotopomers.

Interestingly, upon IR irradiation at 1190 cm^{-1} a simultaneous increase for $C_{60}VO^+$ and decrease for $C_{60}V^+(H_2O)$ is clearly observed (Figure 1b). This may indicate infrared-induced water splitting of $C_{60}V^+(H_2O)$ via

$$C_{60}V^+(H_2O) \rightarrow C_{60}VO^+ + H_2 \quad (3)$$

Such a H_2 loss channel is not a priori expected since i) splitting O–H bonds of an isolated water molecule is a very energy demanding process, ii) a single vanadium atom was found to be incapable of inducing H_2 release from a single water molecule due to a high energy barrier,[8g,j] and iii) the already mentioned infrared photodissociation experiments of $V^+(H_2O)$ clusters have not evidenced such a H_2 loss channel.[12] We calculate the energy requirement of this H_2 release process to be 66 kJ mol^{-1}, which surprisingly is 50 kJ mol^{-1} lower than that of water loss (116 kJ mol^{-1}). The H_2 loss channel is also observed at other wavelengths (Figures 1c, S2, and S3), notably around 1620 cm^{-1}, a frequency characteristic for the water bending vibration. The simultaneous signal loss for $C_{60}V^+(H_2O)$ and growth for $C_{60}VO^+$ in Figure 1c shows that reaction (3) is concurrent for several wavelengths with reaction (1), as evidenced from the in-growth of both $C_{60}VO^+$ and $C_{60}V^+$ in Figures 1b and S3. Although we cannot rule out that an isomer with H_2 is formed already in the source, it should be pointed out that i) a

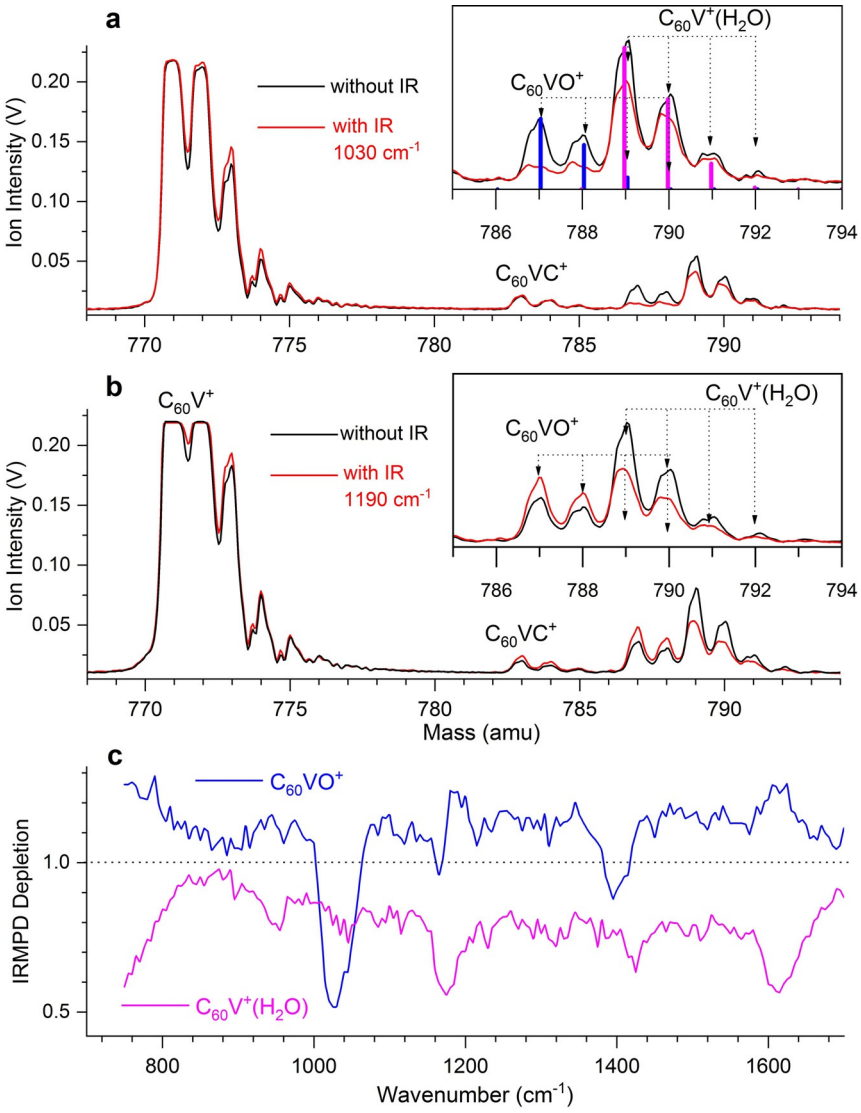

Figure 1. Mass distributions of $C_{60}V^+$, $C_{60}VO^+$, and $C_{60}V^+(H_2O)$ produced via laser vaporization, with (red) and without (black) IR irradiation at 1030 cm^{-1} (panel a) and 1190 cm^{-1} (panel b). Insets of a and b show close-ups of the mass range only covering $C_{60}VO^+$ and $C_{60}V^+(H_2O)$. The simulated natural isotopic distributions of $C_{60}VO^+$ and $C_{60}V^+(H_2O)$ are presented separately in the inset of panel a by blue and pink sticks, respectively. Figures 1a and 1b are from two separate experiments, and the first two isotopes ($m/z = 771$ and 772 amu) of the $C_{60}V^+$ isotopic distribution are saturated because their intensities exceed the data acquisition window. In panel c, IRMPD depletion spectra of $C_{60}VO^+$ (blue trace) and $C_{60}V^+(H_2O)$ (pink trace) show the concurrent $C_{60}VO^+$ signal growth and $C_{60}V^+(H_2O)$ signal loss. The $C_{60}VO^+$ spectrum exhibits a combination of growth due to H_2-loss from $C_{60}V^+(H_2O)$, and loss via $C_{60}VO^+ \rightarrow C_{60} + VO^+$ (most pronounced around 1030 and 1400 cm^{-1}).

maximum depletion of ≈60% was found for $C_{60}V^+(H_2O)$ around 1620 cm^{-1}, suggesting that at least 60% of $C_{60}V^+(H_2O)$ complexes in the molecular beam have an intact water molecule, and ii) the increase of the $C_{60}VO^+$ intensity at 1620 cm^{-1} indicates that the infrared light drives reaction (3) for isomers with an intact water molecule. Infrared-induced chemical reactions have previously been reported by Mackenzie and co-workers for the decomposition of nitrous oxide (N_2O) by rhodium and platinum metal clusters.[18] They demonstrated that such a process could be analogous to temperature programmed desorption experiments on extended surfaces, with the infrared light acting as a source of heat. Given the absence of infrared-induced H_2 loss for the $V^+(H_2O)$ ion,[12] our experimental observation implies that the water splitting process is greatly promoted by the presence of C_{60} in $C_{60}V^+$, which lowers the barrier by more than 70 kJ mol^{-1} as found from following theoretical calculations.

Furthermore, we quantified the signal intensity changes of the dominant isotopomers of $C_{60}V^+$, $C_{60}VO^+$, and $C_{60}V^+(H_2O)$ upon irradiation at 1620 cm^{-1} for $m/z = 771$ (due to detector saturation, derived from $m/z = 773$), 787, and 789 amu, to be +32, +5, and −34 mV, respectively, with an estimated uncertainty of less than 10% (Figure S3a). The summed signal increase of $C_{60}V^+$ and $C_{60}VO^+$ thus roughly equals the signal decrease of $C_{60}V^+(H_2O)$, supporting that a competition between H_2 elimination and H_2O loss occurs at 1620 cm^{-1}. Interestingly, the branching ratio of the H_2 loss channel at 1620 cm^{-1} is estimated to be about 15% of all $C_{60}V^+(H_2O)$ fragmentation, while at 1190 cm^{-1} (Figure 1b) and 760 cm^{-1} (Figure S3b) the branching ratios amount to about 45% and 25%, respectively. This indicates that competition between the H_2O and H_2 loss channels may depend on both the wavelength and the number of absorbed photons at a specific wavelength. This observation suggests that mode-specific excitation could be used to drive the fragmentation dynamics.

To rationalize this observation, we investigated the water splitting mechanism in $C_{60}V^+(H_2O)$, the entrance channel complex of the $C_{60}V^+ + H_2O \rightarrow C_{60}V^+(H_2O) \rightarrow C_{60}VO^+ + H_2$ reaction. To this end, we first focus on understanding the structures of $C_{60}V^+(H_2O)$ and $C_{60}VO^+$. For this, we record the wavelength dependent depletion of $C_{60}V^+(H_2O)$, yielding the IRMPD spectrum of $C_{60}V^+(H_2O)$ as shown in Figure 2a. We have also obtained the IRMPD spectrum of $C_{60}VO^+$ via its depletion through carefully minimizing the in-growth contamination from $C_{60}V^+(H_2O)$ (see discussion below and Figure S4). We then compare the obtained IRMPD spectra with DFT calculated infrared spectra of potential structures.

The IRMPD spectrum of $C_{60}V^+(H_2O)$ displays three intense vibrational bands in the 1000–1700 cm^{-1} spectral range and several low-intensity features that are not well resolved. Therefore, we also recorded the spectrum in this

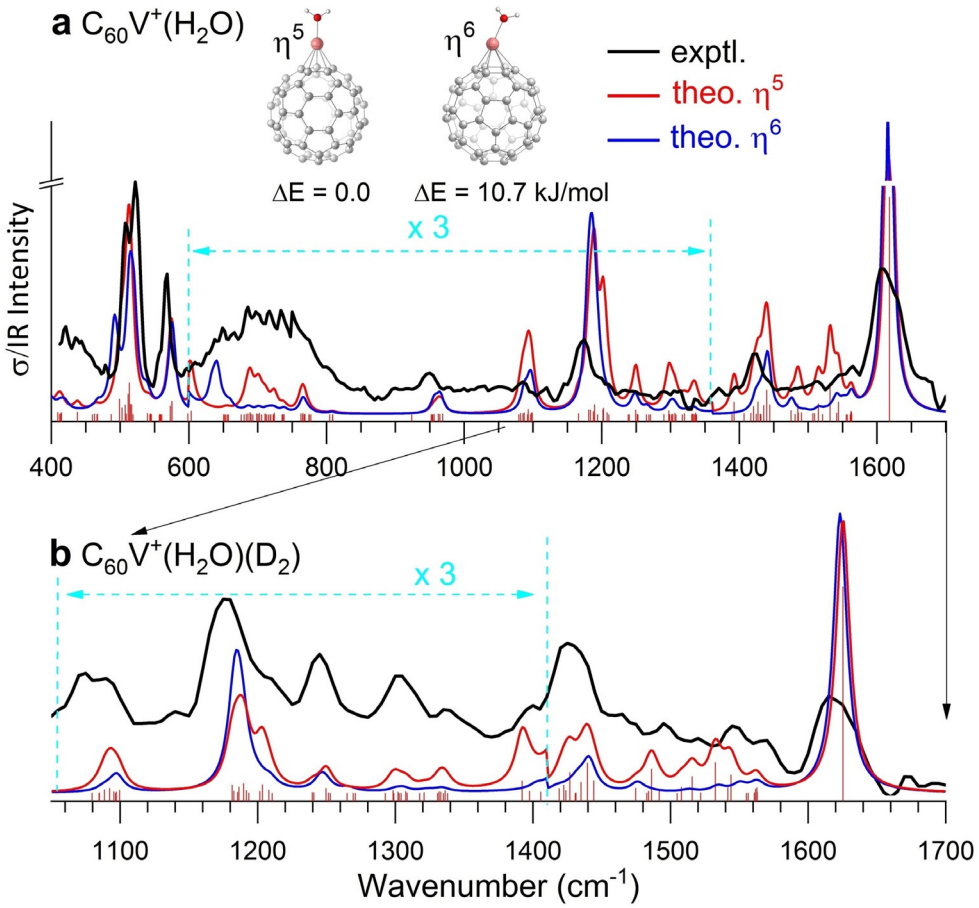

Figure 2. (a) IRMPD spectrum of $C_{60}V^+(H_2O)$ and calculated spectra of $C_{60}V^+(H_2O)$ in η^5 (red) and η^6 (blue) configurations, with their structures and relative stabilities indicated. (b) IRMPD spectrum of $C_{60}V^+(H_2O)(D_2)$ and calculated spectra of the D_2-tagged complexes of η^5 and η^6 $C_{60}V^+(H_2O)$. Calculated spectra are convoluted using Lorentzian line shapes of 12 cm^{-1} full width at half maximum, and the calculated intensities for η^5 are also plotted with sticks. The calculated spectra in the cyan arrowed ranges are multiplied by a factor of three.

range using the D_2-tagging technique, in which the ion of interest is complexed with a D_2 molecule that serves as weakly bound spectator to probe the vibrational structures of $C_{60}V^+(H_2O)$. The calculated binding energy of D_2 to $C_{60}V^+(H_2O)$ is 23 kJ mol^{-1}, or only 2 photons at 1000 cm^{-1}. Monitoring the wavelength dependent depletion of D_2-tagged $C_{60}V^+(H_2O)$ gives the IRMPD spectrum of $C_{60}V^+(H_2O)(D_2)$, as presented in Figure 2b. It closely resembles the spectrum of $C_{60}V^+(H_2O)$ but with the low-intensity spectral features better resolved.

The calculations have yielded two different isomers of $C_{60}V^+(H_2O)$, with $V^+(H_2O)$ binding to pentagon (η^5) or hexagon (η^6) hollow sites. Isomers in which $V^+(H_2O)$ binds to a pentagon-hexagon ($\eta^{2(5-6)}$) bridge site, to a hexagon-hexagon ($\eta^{2(6-6)}$) bridge site, or to an atop (η^1) site, are not stable and converge to either η^5 or η^6. Each isomer can have three spin states, i.e., $S = 2, 1, 0$, corresponding to spin multiplicities of quintet, triplet, and singlet. The η^5 structure (quintet) is calculated to be most stable with the η^6 structure (quintet) 10.7 kJ mol^{-1} higher in energy. We consider both the η^5 and η^6 structures and their D_2-tagged complexes for comparison with the experimental spectra. Calculated spectra for both structures give good matches with the experiment, with that of the η^5 $C_{60}V^+(H_2O)$ arguably slightly better. Nevertheless, the spectra of both isomers indicate that the intense band observed at 1620 cm^{-1} must be attributed to the water bending mode, demonstrating that the water molecule is intact prior to IR irradiation. Such isomers, as discussed above, constitute at least 60% of the $C_{60}V^+(H_2O)$ complexes. The band at 1620 cm^{-1} is also seen in the IRMPD spectrum of $C_{60}V^+(H_2O)(D_2)$ and is again excellently reproduced by the theoretical calculations. It is noted that the bending frequency of H_2O in $C_{60}V^+(H_2O)$ (ca. 1618 cm^{-1}) has red-shifted by 20 and 8 cm^{-1} compared to the calculated values of free H_2O and $V^+(H_2O)$, respectively, indicating that water is slightly activated in the complex. This is consistent with the slightly elongated O–H bond length in $C_{60}V^+(H_2O)$ (0.98 Å) compared to free water (0.97 Å), but it is marginally shorter than in $V^+(H_2O)$ by a mere 0.001 Å. The other bands are mainly C_{60} vibrations, which have been perturbed by the adsorbed V^+ and H_2O. A notable exception is the intense feature at about 510 cm^{-1} which involves the dangling motion of the water molecule around the $C_{60}V^+$ framework (Figure S5).

We now consider the structure of the $C_{60}VO^+$ product. It is well-established that VO^+ has a $^3\Sigma$ ground state. Since C_{60} is a closed-shell molecule, it is expected that $C_{60}VO^+$ has also a $^3\Sigma$ ground state. Indeed, our calculations predict that the triplet state is over 100 kJ mol^{-1} more stable than the quintet state for both η^5 and η^6 $C_{60}VO^+$. The IRMPD spectrum of $C_{60}VO^+$ is dominated by a band around 1030 cm^{-1} that is assigned to the V–O stretching vibration (Figures S4 and S5). The comparison between our calculations and the experimental spectrum of $C_{60}VO^+$ in the 800–1700 cm^{-1} range suggests that both η^5 and η^6 $C_{60}VO^+$ could be present in the experiment, with η^6 more stable by 15 kJ mol^{-1}.

With the structures of $C_{60}V^+(H_2O)$ and $C_{60}VO^+$ validated, Figure 3b presents the calculated reaction potential energy surface (PES) for $C_{60}V^+ + H_2O \rightarrow C_{60}V^+(H_2O) \rightarrow C_{60}VO^+ + H_2$ using η^5 $C_{60}V^+$ as starting point. Both quintet and triplet reaction pathways have been considered in the calculations. An equivalent PES using η^6 $C_{60}V^+$ as starting point is

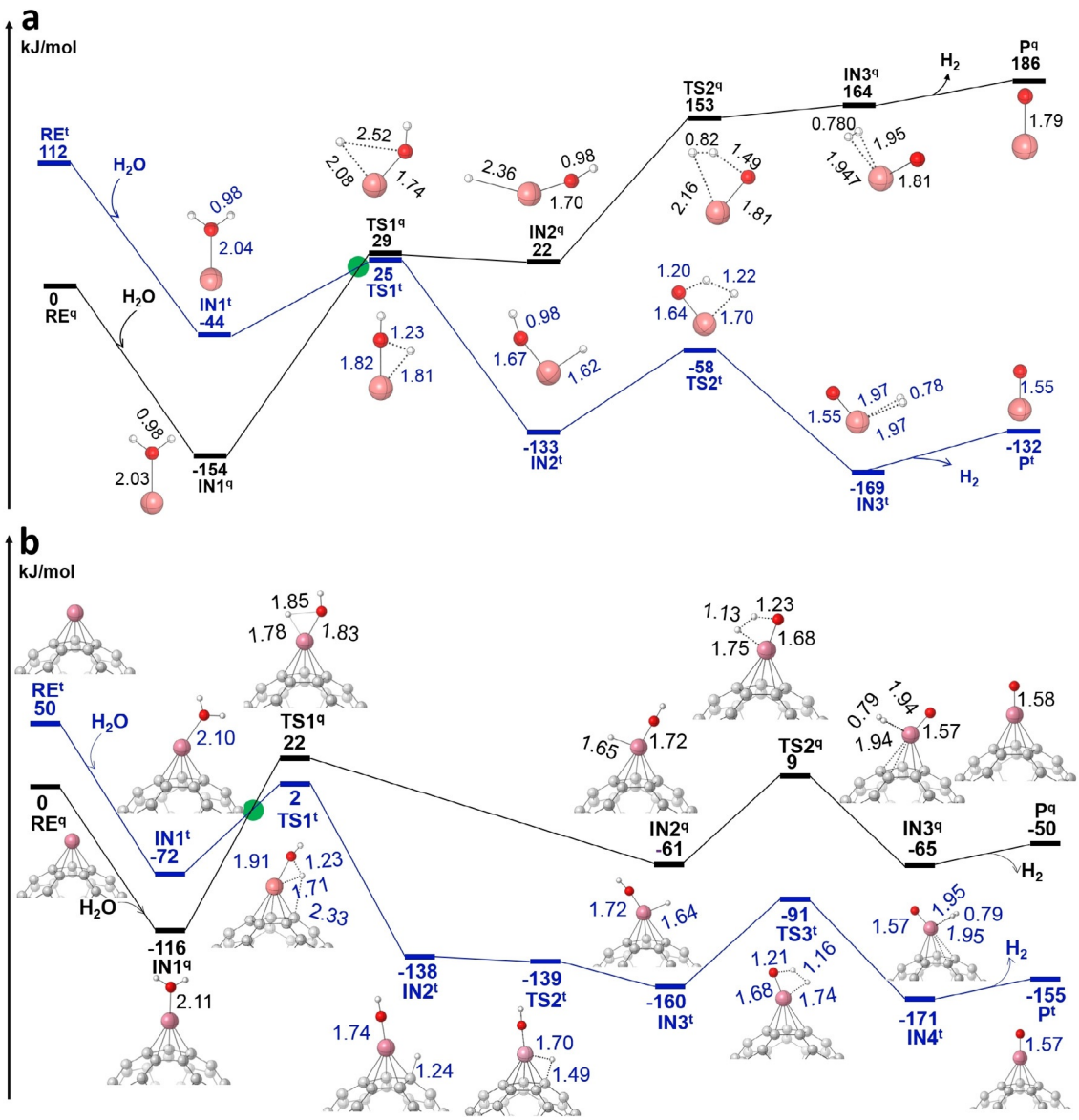

Figure 3. Calculated reaction potential energy surfaces (PESs) for (a) $V^+ + H_2O \rightarrow V^+(H_2O) \rightarrow VO^+ + H_2$ and (b) $C_{60}V^+ + H_2O \rightarrow C_{60}V^+(H_2O) \rightarrow C_{60}VO^+ + H_2$ with η^5 $C_{60}V^+$ as starting point at BPW91/6–311++G(2df,2p)//6–31G(d,p) level of theory. Both quintet (black) and triplet (blue) surfaces are shown. The various states are denominated with RE for reactant, IN for reaction intermediate, TS for transition state, and P for product, and labeled with a superscript *t* and *q*, for triplet or quintet, respectively. The quintet-to-triplet spin-crossing points, i.e., the Minimum Energy Crossing Points (MECPs), are schematically indicated with green circles at the crossings of the two potential energy surfaces. Key bond lengths are indicated in Å. All energies are given with respect to those of the reactants on the quintet surface.

provided in Figure S6, showing a similar reaction pathway and energetics as that based on η^5 $C_{60}V^+$. To better understand the role of the C_{60} support in the reaction, the water splitting reaction pathway by a single V^+ atom is also calculated (Figure 3a) for comparison. In general, our calculated reaction PES for $V^+ + H_2O \rightarrow VO^+ + H_2$ agrees well with previous theoretical and experimental work on this reaction.[13b,c]

The reaction between $C_{60}V^+$ and H_2O is initiated via the formation of entrance channel ion-molecule complex, i.e., $C_{60}V^+(H_2O)$. The V–O distances in $C_{60}V^+(H_2O)$ are 2.11 and 2.10 Å in the quintet (**IN1^q**) and triplet (**IN1^t**) states, respectively, which are much longer than the V–O distances (2.03 and 2.04 Å) in their $V^+(H_2O)$ counterparts. The first transition states (**TS1^q** and **TS1^t**) along both quintet and triplet reaction pathways are characterized by a hydrogen transfer from the oxygen to the metal. In **TS1^q**, the transferred H remains relatively far away from the C_{60} surface, while in **TS1^t** it leans over to the C_{60} surface. **TS1^q** lies about 20 kJ mol^{-1} above **TS1^t**, and **TS1^t** is only marginally higher (+2 kJ mol^{-1}) than the total energies of reactants quintet $C_{60}V^+$ and H_2O. Comparison with the reaction PES for the bare V^+ ion shows that the C_{60} support significantly changes the energy difference between the quintet and triplet surfaces: for the reactants it is reduced from about 110 kJ mol^{-1} for the bare ion to less than 50 kJ mol^{-1} when C_{60} is present, and the same holds for the entrance complexes. This makes the quintet-to-triplet spin-crossing via the Mini-

mum Energy Crossing Point (MECP) much more accessible, because **TS1^t** now lies 20 kJ mol^{-1} below **TS1^q** where it is only 4 kJ mol^{-1} for the reaction between bare V^+ and H_2O. Such spin-crossing makes the transition state a mere 2 kJ mol^{-1} above the reactants when C_{60} is present, but it is 25 kJ mol^{-1} without C_{60} support. This surmised spin-crossing is critical to allow the quintet reactant surface to "switch" into a triplet reaction product surface, which otherwise is a spin-forbidden process according to the Wigner-Witmer spin-conservation rules.[19] It reduces the energy barrier substantially from 179 kJ mol^{-1} for the $V^+ + H_2O$ reaction to 118 kJ mol^{-1} for the $C_{60}V^+ + H_2O$ reaction. Most interestingly, the C_{60} support seems to act as a "hydrogen shuttle" to temporally store the transferred H atom on its surface via covalent C–H interaction (Figure 4), and then the H atom transfers back to V via an essentially barrierless process (**IN2^t** to **IN3^t** via **TS2^t**). This step is important, as it greatly facilitates the formation of the $C_{60}VO^+(H_2)$ intermediate (**IN4^t**) via an energy barrier of 69 kJ mol^{-1}. This barrier is lower than that of the $V^+ + H_2O$ reaction in forming the $VO^+(H_2)$ intermediate (75 kJ mol^{-1}). to the reaction then ends, forming the triplet $C_{60}VO^+$ product concomitant with the release of H_2.

Next, we try to understand, through analyzing the orbital interactions, how the C_{60} support substantially reduces the energy barrier of the first step of the reaction. Figure 4 shows that in **TS1^t** of the $V^+ + H_2O$ reaction, there is orbital overlap between the d_{z2} of the metal center and the 1s orbital of the transferred hydrogen in H_2O; while in **TS1^t** of the $C_{60}V^+ + H_2O$ reaction, the orbital overlap further extends to the 2p orbital of one carbon in C_{60}. That overlap with the 2p orbital of carbon substantially stabilizes the transition state (**TS1^t**). To further disclose the support (C_{60}) effect on the energy barrier, the NBO partial charges have been calculated (Table S1). In **IN1^q** of the $C_{60}V^+ + H_2O$ reaction, almost no charge transfer occurs between C_{60} and $V^+(H_2O)$, leading to similar charges as in **IN1^q** of the $V^+ + H_2O$ reaction. However, in **TS1^t** of the $C_{60}V^+ + H_2O$ reaction, 0.19 *e* has been transferred from C_{60} to $V^+(H_2O)$, exhibiting the stabilization effect of C_{60}. Specifically, the positive charge of V decreases from 0.86 *e* (**IN1^q**) to 0.71 *e* (**TS1^t**) for the $C_{60}V^+ + H_2O$ reaction, while it increases from 0.92 *e* (**IN1^q**) to 1.09 *e* (**TS1^t**) for the $V^+ + H_2O$ reaction, showing an opposite trend. The barrier reduction is further semi-quantified by calculating the single point energy difference of $V^+(H_2O)$ moieties with their geometries same as in **IN1^q** and **TS1^t** of the $C_{60}V^+ + H_2O$ reaction, which amounts to 191 kJ mol^{-1}, while the "true" energy barrier is only 118 kJ mol^{-1}, lower by 73 kJ mol^{-1}.

Conclusion

In conclusion, we studied the water splitting reaction by a single vanadium cation supported on C_{60}. The entrance channel complex $C_{60}V^+(H_2O)$ and the end product $C_{60}VO^+$ of the reaction have been characterized by infrared multiple photon dissociation spectroscopy, and their structures are investigated through comparisons with density functional theory calculations. The detailed reaction mechanism of water splitting by $C_{60}V^+$ was explored, and a pronounced support effect was found. C_{60} reduces the reaction barrier compared to the same reaction without C_{60}, i.e., water splitting by V^+. The NBO partial charge and orbital interaction analyses reveal that the reaction barrier is reduced because there is charge transfer from the support to vanadium, and the orbital overlap between the first transferred hydrogen of water and the metal center extends to one carbon atom of the C_{60}. Both the charge transfer and orbital overlap serve to stabilize the transition state, thus lowering its energy difference (reducing the energy barrier) with the entrance channel complex. This work demonstrates the significant effect of carbon support in water splitting reactions and contributes to the understanding of the catalytic properties of porous carbon material based single atom catalysts.

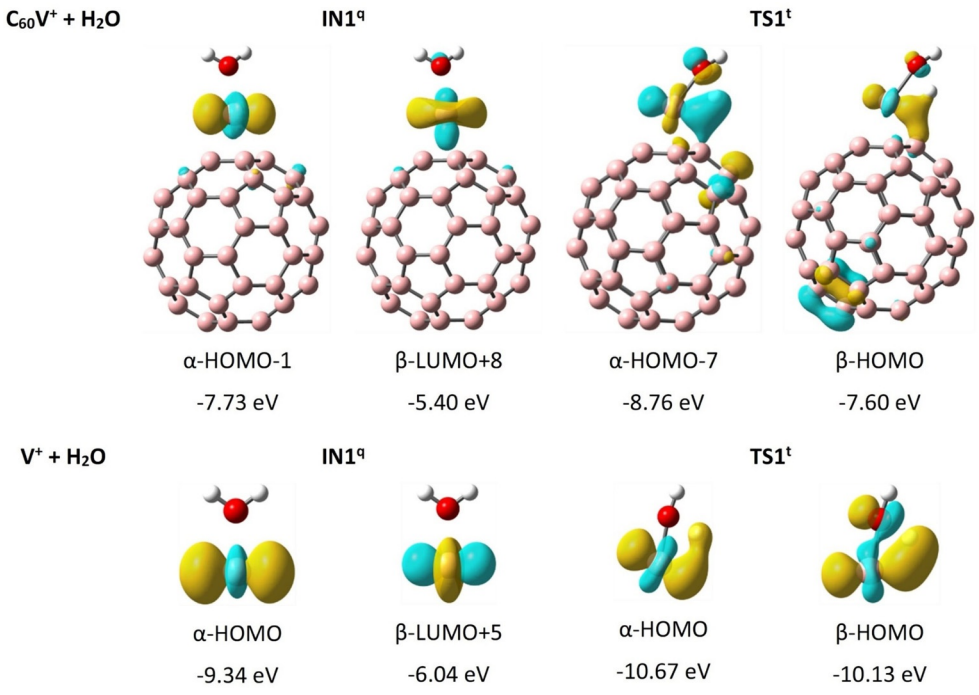

Figure 4. Frontier molecular orbitals (isovalue = 0.04 a.u.) of the **IN1^q** (quintet) and **TS1^t** (triplet) of the water-splitting reaction that show orbital overlap between V and the transferred H of water. HOMO: highest occupied molecular orbital; LUMO: lowest unoccupied molecular orbital.

Acknowledgements

This work was supported by the KU Leuven Research Council (Project No. C14/18/073) and by the European Union's Framework Programme Horizon 2020 via project Catchy under the Marie Skłodowska-Curie grant agreement 955650 and project CALIPSOplus grant agreement 730872. The theoretical calculations is supported by National Natural Science Foundation of China (22003048, U1866203, and 11674263). Part of the computational resources and services were also provided by the VSC (Flemish Supercomputer Center), funded by the Research Foundation-Flanders (FWO) and the Flemish Government-department EWI. We gratefully acknowledge the Nederlandse Organisatie voor Wetenschappelijk Onderzoek (NWO) for the support of the FELIX Laboratory and thank the FELIX staff. P.F. acknowledges the FWO for a senior postdoctoral grant. Additionally, we are grateful to Prof. J. N. Harvey (KU Leuven) for valuable discussions on the spin crossing.

Conflict of Interest

The authors declare no conflict of interest.

Keywords: C_{60} · metal–support interaction · single atom catalysis · single vanadium · water splitting

[1] a) J. Yang, A. Sudik, C. Wolverton, D. J. Siegel, *Chem. Soc. Rev.* **2010**, *39*, 656 – 675; b) J. Vanbuel, P. Ferrari, E. Janssens, *Adv. Phys. X* **2020**, *5*, 1754132.

[2] J. D. Blakemore, R. H. Crabtree, G. W. Brudvig, *Chem. Rev.* **2015**, *115*, 12974 – 13005.

[3] a) X. Zou, Y. Zhang, *Chem. Sco. Rev.* **2015**, *44*, 5148 – 5180; b) M. M. Najafpour, G. Renger, M. Hołyńska, A. N. Moghaddam, E.-M. Aro, R. Carpentier, H. Nishihara, J. J. Eaton-Rye, J.-R. Shen, S. I. Allakhverdiev, *Chem. Rev.* **2016**, *116*, 2886 – 2936.

[4] a) X.-F. Yang, A. Wang, B. Qiao, J. Li, J. Liu, T. Zhang, *Acc. Chem. Res.* **2013**, *46*, 1740 – 1748; b) J. Liu, *ACS Catal.* **2017**, *7*, 34 – 59; c) J.-C. Liu, Y. Tang, Y.-G. Wang, T. Zhang, J. Li, *Natl. Sci. Rev.* **2018**, *5*, 638 – 641; d) H.-Y. Zhuo, X. Zhang, J.-X. Liang, Q. Yu, H. Xiao, J. Li, *Chem. Rev.* **2020**, *120*, 12315 – 12341; e) S. K. Kaiser, Z. Chen, D. F. Akl, S. Mitchell, J. Pérez-Ramírez, *Chem. Rev.* **2020**, *120*, 11703 – 11809; f) R. Lang, X. Du, Y. Huang, X. Jiang, Q. Zhang, Y. Guo, K. Liu, B. Qiao, A. Wang, T. Zhang, *Chem. Rev.* **2020**, *120*, 11986 – 12043.

[5] B. Qiao, A. Wang, X. Yang, L. F. Allard, Z. Jiang, Y. Cui, J. Liu, J. Li, T. Zhang, *Nat. Chem.* **2011**, *3*, 634 – 641.

[6] Y.-G. Wang, D. Mei, V.-A. Glezakou, J. Li, R. Rousseau, *Nat. Commun.* **2015**, *6*, 6511.

[7] a) C. Zhu, Q. Shi, S. Feng, D. Du, Y. Lin, *ACS Energy Lett.* **2018**, *3*, 1713 – 1721; b) J. Deng, H. Li, J. Xiao, Y. Tu, D. Deng, H. Yang, H. Tian, J. Li, P. Ren, X. Bao, *Energy Environ. Sci.* **2015**, *8*, 1594 – 1601; c) C. Ling, L. Shi, Y. Ouyang, X. C. Zeng, J. Wang, *Nano Lett.* **2017**, *17*, 5133 – 5139; d) N. Cheng, S. Stambula, D. Wang, M. N. Banis, J. Liu, A. Riese, B. Xiao, R. Li, T.-K. Sham, L.-M. Liu, G. A. Botton, X. Sun, *Nat. Commun.* **2016**, *7*, 13638.

[8] a) K. R. Asmis, A. Fielicke, *Top. Catal.* **2018**, *61*, 1 – 2; b) P. Ferrari, L. M. Molina, V. Kaydashev, J. A. Alonso, P. Lievens, E. Janssens, *Angew. Chem. Int. Ed.* **2016**, *55*, 11059 – 11063; *Angew. Chem.* **2016**, *128*, 11225 – 11229; c) M. Jia, J. Vanbuel, P. Ferrari, E. M. Fernández, S. Gewinner, W. Schöllkopf, M. T. Nguyen, A. Fielicke, E. Janssens, *J. Phys. Chem. C* **2018**, *122*, 18247 – 18255; d) J. Vanbuel, M.-Y. Jia, P. Ferrari, S. Gewinner, W. Schöllkopf, M. T. Nguyen, A. Fielicke, E. Janssens, *Top. Catal.* **2018**, *61*, 62 – 70; e) Y. X. Zhao, Z. Y. Li, Y. Yang, S. G. He, *Acc. Chem. Res.* **2018**, *51*, 2603 – 2610; f) E. Janssens, H. T. Le, P. Lievens, *Chem. Eur. J.* **2015**, *21*, 15256 – 15262; g) H. Zhang, H. Wu, Y. Jia, B. Yin, L. Geng, Z. Luo, K. Hansen, *Commun. Chem.* **2020**, *3*, 148; h) Y.-X. Zhao, B. Yang, H.-F. Li, Y. Zhang, Y. Yang, Q.-Y. Liu, H.-G. Xu, W.-J. Zheng, S.-G. He, *Angew. Chem. Int. Ed.* **2020**, *59*, 21216 – 21223; *Angew. Chem.* **2020**, *132*, 21402 – 21409; i) G.-L. Hou, E. Faragó, D. Buzsáki, L. Nyulászi, T. Höltzl, E. Janssens, *Angew. Chem. Int. Ed.* **2021**, *60*, 4756 – 4763; *Angew. Chem.* **2021**, *133*, 4806 – 4813; j) H. Zhang, M. Zhang, Y. Jia, L. Geng, B. Yin, S. Li, Z. Luo, F. Pan, *J. Phys. Chem. Lett.* **2021**, *12*, 1593 – 1600.

[9] a) S. M. Lang, I. Fleischer, T. M. Bernhardt, R. N. Barnett, U. Landman, *Nano Lett.* **2013**, *13*, 5549 – 5555; b) S. M. Lang, T. M. Bernhardt, D. M. Kiawi, J. M. Bakker, R. N. Barnett, U. Landman, *Angew. Chem. Int. Ed.* **2015**, *54*, 15113 – 15117; *Angew. Chem.* **2015**, *127*, 15328 – 15332; c) S. M. Lang, T. M. Bernhardt, D. M. Kiawi, J. M. Bakker, R. N. Barnett, U. Landman, *Phys. Chem. Chem. Phys.* **2016**, *18*, 15727 – 15737.

[10] M. R. Fagiani, X. Song, S. Debnath, S. Gewinner, W. Schöllkopf, K. R. Asmis, F. A. Bischoff, F. Muller, J. Sauer, *J. Phys. Chem. Lett.* **2017**, *8*, 1272 – 1277.

[11] G. Liu, E. Miliordos, S. Ciborowski, M. Tschurl, U. Boesl, U. Heiz, X. Zhang, S. Xantheas, K. Bowen, *J. Chem. Phys.* **2018**, *149*, 221101.

[12] a) N. R. Walker, R. S. Walters, E. D. Pillai, M. A. Duncan, *J. Chem. Phys.* **2003**, *119*, 10471 – 10474; b) P. D. Carnegie, J. H. Marks, A. D. Brathwaite, T. B. Ward, M. A. Duncan, *J. Phys. Chem. A* **2020**, *124*, 1093 – 1103.

[13] a) D. E. Clemmer, Y.-M. Chen, N. Aristov, P. B. Armentrout, *J. Phys. Chem.* **1994**, *98*, 7538 – 7544; b) A. Irigoras, J. E. Fowler, J. M. Ugalde, *J. Am. Chem. Soc.* **1999**, *121*, 574 – 580; c) Y. Xu, Y.-C. Chang, M. Parziale, A. Wannenmacher, C.-Y. Ng, *J. Phys. Chem. A* **2020**, *124*, 8884 – 8896.

[14] B. S. Fox, I. Balteanu, O. P. Balaj, H. Liu, M. K. Beyer, V. E. Bondybey, *Phys. Chem. Chem. Phys.* **2002**, *4*, 2224 – 2228.

[15] a) B. Scharfschwerdt, C. van der Linde, O. P. Balaj, I. Herber, D. Schütze, M. K. Beyer, *Low Temp. Phys.* **2012**, *38*, 717 – 722; b) J. Heller, T. F. Pascher, D. Muß, C. van der Linde, M. K. Beyer, M. Ončák, *Phys. Chem. Chem. Phys.* **2021**, *23*, 22251 – 22262.

[16] a) J. Zhu, Y. Huang, W. Mei, C. Zhao, C. Zhang, J. Zhang, I. S. Amiinu, S. Mu, *Angew. Chem. Int. Ed.* **2019**, *58*, 3859 – 3864; *Angew. Chem.* **2019**, *131*, 3899 – 3904; b) M. Chen, S. Wang, H. Zhang, P. Zhang, Z. Tian, M. Lu, X. Xie, L. Huang, W. Huang, *Nano Res.* **2020**, *13*, 729 – 735.

[17] D. M. Merriles, A. Sevy, C. Nielson, M. D. Morse, *J. Chem. Phys.* **2020**, *153*, 024303.

[18] a) S. M. Hamilton, W. S. Hopkins, D. J. Harding, T. R. Walsh, P. Gruene, M. Haertelt, A. Fielicke, G. Meijer, S. R. Mackenzie, *J. Am. Chem. Soc.* **2010**, *132*, 1448 – 1449; b) S. M. Hamilton, W. S. Hopkins, D. J. Harding, T. R. Walsh, M. Haertelt, C. Kerpal, P. Gruene, G. Meijer, A. Fielicke, S. R. Mackenzie, *J. Phys. Chem. A* **2011**, *115*, 2489 – 2497; c) I. S. Parry, A. Kartouzian, S. M. Hamilton, O. P. Balaj, M. K. Beyer, S. R. Mackenzie, *Angew. Chem. Int. Ed.* **2015**, *54*, 1357 – 1360; *Angew. Chem.* **2015**, *127*, 1373 – 1377; d) G. Meizyte, A. E. Green, A. S. Gentleman, S. Schaller, W. Schöllkopf, A. Fielicke, S. R. Mackenzie, *Phys. Chem. Chem. Phys.* **2020**, *22*, 18606 – 18613.

[19] H. Schwarz, *Int. J. Mass Spectrom.* **2004**, *237*, 75 – 105.

Manuscript received: September 12, 2021
Accepted manuscript online: October 5, 2021
Version of record online: November 10, 2021

